# Soft Matter



**PAPER** 

**View Article Online** 



Cite this: Soft Matter, 2022. 18, 6340

remodeling in hydrogels with a step-change in elastic modulus†

Measuring human mesenchymal stem cell

John A. McGlynn and Kelly M. Schultz 10 \*

Human mesenchymal stem cells (hMSCs) are instrumental in the wound healing process. They migrate to wounds from their native niche in response to chemical signals released during the inflammatory phase of healing. At the wound, hMSCs downregulate inflammation and regulate tissue regeneration. Delivering additional hMSCs to wounds using cell-laden implantable hydrogels has the potential to improve healing outcomes and restart healing in chronic wounds. For these materials to be effective, cells must migrate from the scaffold into the native tissue. This requires cells to traverse a step-change in material properties at the implant-tissue interface. Migration of cells in material with highly varying properties is not well characterized. We measure 3D encapsulated hMSC migration and remodeling in a well-characterized hydrogel with a step-change in stiffness. This cell-degradable hydrogel is composed of 4-arm poly(ethylene glycol)-norbornene cross-linked with an enzymatically-degradable peptide. The scaffold is made with two halves of different stiffnesses separated by an interface where stiffness changes rapidly. We characterize changes in structure and rheology of the pericellular region using multiple particle tracking microrheology (MPT). MPT measures Brownian motion of embedded particles and relates it to material rheology. We measure more remodeling in the soft region of the hydrogel than the stiff region on day 1 post-encapsulation and similar remodeling everywhere on day 6. In the interface region, we measure hMSC-mediated remodeling along the interface and migration towards the stiff side of the scaffold. These results can improve materials designed for cell delivery from implants to a wound to enhance healing.

Received 31st May 2022, Accepted 8th August 2022

DOI: 10.1039/d2sm00717a

rsc.li/soft-matter-journal

### 1 Introduction

Human mesenchymal stem cells (hMSCs) are important cells in the wound healing process.<sup>1-7</sup> They migrate to an injury site in response to chemical signals released from the wound. 2,6,7 During migration, they actively remodel their surroundings both irreversibly using enzymes called matrix metalloproteinases (MMPs) and reversibly by applying force to the network. MMPs and cellularly applied forces change the structure of the cell's surroundings. The material around the cell affected by this activity we define as our pericellular region.8-11 This remodeling significantly changes the material structure and rheology.<sup>12</sup> Once they reach the wound, they are part of directing the healing process through the final three stages. They do this in a variety of ways, including regulating inflammation, recruiting other cells to repair tissue and reorganizing collagen.<sup>2,6,7</sup>

Department of Chemical and Biomolecular Engineering, Lehigh University, Iacocca Hall, 111 Research Drive, Bethlehem, PA, USA, E-mail; kes513@lehigh.edu; Tel: +610 758-2012

† Electronic supplementary information (ESI) available. See DOI: https://doi.org/ 10.1039/d2sm007179

Because of the ability of hMSCs to enhance wound repair, implantable materials which encapsulate and deliver additional hMSCs to a wound are being designed. 13-22 In order for these materials to be effective, encapsulated hMSCs must retain normal function within the implanted scaffold and migrate out of it and into the native tissue to participate in wound repair. During this migration, hMSCs will traverse a step-change in properties as they leave the implanted material and enter native tissue. Understanding how hMSCs interact with materials with a rapid change in properties is critical when designing scaffolds that effectively deliver hMSCs to wounds. In this work, we characterize hMSC migration and remodeling in a welldefined polymer-peptide hydrogel with a step-change in elastic

Previous work has shown that hMSC motility, lineage specification and morphology are significantly affected by the stiffness and cross-link density of their surroundings. 13,23-25 These changes in structure, specifically step-changes, can be encountered naturally in the body and between an implanted hydrogel and native tissue. Human joints consist of a layer of cartilage joined to bone by a layer of rapidly increasing calcification ranging from 20-250 µm thick, forming a gradient in

**Paper** 

stiffness.<sup>26</sup> In the event of an injury to the cartilage layer, cells

will need to migrate across the stiff mineralized cartilage to repair the tissue.<sup>26</sup> Kar et al. showed that hMSCs encapsulated in degradable hydrogels implanted into mice initially did not traverse the implant-tissue interface preventing migration out of the scaffold. Cells needed to degrade the hydrogel significantly for 48-72 hours before they could cross the interface and migrate into native tissue.<sup>27</sup> Additionally, cells leave the hydrogel more rapidly when the material is quickly degraded and remodeled.<sup>27</sup> This shows the importance of understanding how encapsulated cells remodel an interface prior to migration when designing implantable hydrogels as cell delivery vehicles.

A variety of hydrogel biomaterials have been used to encapsulate cells, many of which can be easily fabricated with variable stiffness. 13,15,20,22,28-30 One common method of creating a hydrogel with a step-change in stiffness is to use a photomask to vary UV light exposure in different regions of the photopolymerizerable polymer precursor solution to spatially change the degree of crosslinking and stiffness. 19,31,32 Once polymerized, this hydrogel will have two regions of constant stiffness separated by an interface. We call these scaffolds "interface" hydrogels. Marklein and Burdick fabricated hydrogels with a series of strips with alternating stiffnesses using this method.31 They seeded hMSCs on these materials in 2D and showed that cells on stiffer regions spread and had higher cell areas while those on the softer material did not spread as effectively. This demonstrates that cell morphology can be controlled with material stiffness and is important because cell shape is a factor that determines motility. In this work, we 3D encapsulate hMSCs in a well-defined PEG-based hydrogel scaffold that cross-links with an MMP-degradable peptide when exposed to UV light in the presence of a photoinitiator. 13,15,33,34 This material has been widely used to study cell-material interactions. 8,10,12,15,34,35 We recently showed that this hydrogel can be fabricated with a step-change in mechanical stiffness by varying UV light exposure.36 This work focuses on how individual cells remodel and degrade material in response to rapid changes in their microenvironment. While previous work has characterized motility and morphology of hMSCs in non-uniform hydrogels, most of these studies are done in 2-dimensions with cells seeded on top of hydrogels. 19,24,37 Additionally, most studies do not characterize the local cell-mediated material remodeling in response to sharp changes in mechanical properties, instead focusing on measuring cell morphology and bulk material degradation. 19,31,38 In order to characterize changes in material properties in pericellular regions around migrating cells in response to step-changes in material stiffness, we use multiple particle tracking microrheology.

Multiple particle tracking microrheology (MPT) is a passive microrheological technique that measures the Brownian motion of probe particles embedded in a material to characterize its structure and rheology. 33,39,40 Particles are tracked and the meansquared displacement (MSD,  $\langle \Delta r^2(\tau) \rangle$ ) is related to material properties using the Generalized Stokes-Einstein Relation (GSER). 33,39,41,42

The logarithmic slope of the MSD,  $\alpha = \frac{d \; \log \langle \Delta r^2(\tau) \rangle}{d \; \log \tau}$ , quantitatively identifies the state of the material. hMSC remodeling creates a

spatially heterogeneous and constantly evolving cellular microenvironment, using cell-secreted MMPs and cytoskeletal tension, which affects migration.<sup>8,10,12,43</sup> A distinct advantage of microrheology is its ability to characterize the rheology of heterogeneous material and measure spatially varying properties by splitting the field of view into different sections and analyzing them separately for their rheological properties. This makes MPT a powerful characterization technique for this work. We use MPT to measure the remodeling of the pericellular region around individual migrating cells. We quantify cellmediated remodeling based on the position of the cell in the hydrogel relative to the interface.

In this work, we encapsulate hMSCs in a polymer-peptide hydrogel with an interface in stiffness. We characterize cellmediated pericellular remodeling in different 500 µm wide sections of the hydrogel relative to the interface. Cells are characterized in either the soft, stiff or interface region. We measure that on day 1 post-encapsulation, more remodeling occurs in the soft half of the hydrogel than in other areas of the scaffold. On day 6 post-encapsulation, we measure more remodeling in the stiff half of the hydrogel when compared to the same region days 1 and 2 post-encapsulation, with most cells in the hydrogel remodeling past the gel-sol transition. We quantify the persistence of hMSCs in all regions of the gel. On days 1 and 2 post-encapsulation, cells are not persistent and migrate randomly in every region of the hydrogel. On day 6 postencapsulation, cells in the interface region migrate towards the stiff half while those in the soft and stiff halves migrate randomly. Finally, we characterize spatial variations in pericellular rheology in each region of the hydrogel. We measure that cells create a gradient in degradation in their pericellular region with the gradient in stiffness in the interface. Degradation profiles measured in the soft and stiff regions agree with previous literature. This work provides a detailed look at how hMSCs remodel and migrate through an interface in stiffness similar to one which might be present as they exit an implanted hydrogel and enter the wound. These quantitative results can inform design of new materials that use the physical microenvironment to manipulate the direction of cell migration out of the scaffold to increase delivery.

# 2 Materials and methods

#### 2.1 Hydrogel composition

The hydrogel scaffold used in this work is composed of a 4-arm poly(ethylene glycol)-norbornene backbone (PEG-N, 3 mM,  $M_{\rm n} = 20\,000 \text{ g mol}^{-1}, f = 4 \text{ where } f \text{ is the number of functional}$ groups, JenKem Technology) cross-linked with an MMPdegradable peptide (KCGPQG  $\downarrow$  IWGQCK, 3.9 mM,  $M_n$  = 1305 g mol<sup>-1</sup>, f = 2, Bachem). This peptide is cleaved by cellsecreted MMPs allowing encapsulated cells to irreversibly degrade and remodel their surroundings.44-46 We also include a cellular adhesion peptide, CRGDS (1 mM,  $M_n = 594 \text{ g mol}^{-1}$ , f=1, American Peptide Inc.), which enables cellular attachment to the network. 15 The thiols in the cysteines react with the -ene groups in the norbornene during UV light exposure in the presence of a photoinitiator, lithium phenyl-2,4,6-trimethylbenzoyl-phosphinate (LAP, 1.7 mM), to create a chemically cross-linked network with tethered adhesion peptides.<sup>47</sup> LAP is synthesized using previously published protocols.<sup>47</sup>

1 µm fluorescently labeled carboxylated polystyrene probe particles ( $2a = 0.97 \pm 0.01 \mu m$ , where a is the particle radius, 0.2% solids volume<sup>-1</sup>, Polysciences) are included in the precursor solution to enable MPT measurements. This concentration of particles is used to ensure that enough particles are in the field of view (160  $\times$  160  $\mu$ m) for statistical accuracy in the MSD (approximately 50-100 particles) while also preventing particle-particle interaction and minimizing aggregation.<sup>33,39</sup> Prior to use in an experiment, particles are washed by centrifugation (Eppendorf centrifuge 5424) at 5000 RPM and resuspended in fresh deionized water. This removes any unreacted fluorescent molecules and debris present in the stock probe particle solution. We use this washing procedure to wash the particles 2 more times, then the particles are sonicated (Branson CPX1800) for at least 15 min to break up any aggregates which may have formed during washing. hMSCs are also included in the polymer precursor solution prior to photopolymerization. Details of this are provided in the next section.

#### 2.2 Cell culture

Human mesenchymal stem cells (hMSCs) are acquired in passage 2 from Lonza. They are plated on 150 cm $^2$  tissue culture Petri dishes (Corning) that are filled with 30–60 mL of growth media. Growth media is composed of 90% Dulbecco's modified Eagle medium (DMEM, Life Technologies), 10% fetal bovine serum (FBS, Life Technologies), 50 U mL $^{-1}$  penicillin/streptomycin (Life Technologies), 0.5  $\mu$ g mL $^{-1}$  fungizone (Life Technologies) and 1 ng mL $^{-1}$  human fibroblast growth factor (hFGF, Peprotech).

To encapsulate cells in a hydrogel, hMSCs are removed from the Petri dish using 8 mL of trypsin–EDTA (0.125%, Thermo Fisher Scientific). Cells are then centrifuged and resuspended in phosphate buffered saline (1× PBS, Gibco). They are counted using a hemocytometer (VWR) and added to the precursor solution of hydrogel components at a final concentration of 2  $\times$  10 $^5$  cells mL $^{-1}$ . This low cell concentration is used to minimize cell–cell interactions in our material.

#### 2.3 Sample chamber

The sample chamber used in this work is composed of a glass-bottomed Petri dish (D=35 mm where D is the diameter, Ibidi GmbH) and a polydimethylsiloxane (PDMS, SYLGARD 184, Dow Corning) ring. The ring is used to prevent translation of the sample during an experiment. Rings are made from a flat sheet of PDMS formed by mixing 90% elastomer with 10% curing agent, as recommended by the manufacturer. This mixture is degassed and reacted overnight at 65 °C in a Petri dish as a flat sheet. After complete reaction, a ring with an inner diameter of 6 mm, an outer diameter of 10 mm and a height of  $\approx$  6 mm is cut from the flat PDMS sheet using biopsy punches (Integra Bioscience).

The PDMS ring is attached to the glass-bottomed Petri dish using uncured PDMS. Petri dishes are placed in an oven overnight at 65  $^{\circ}$ C to attach the PDMS ring and then sterilized using 70% ethanol prior to use in a cell experiment. The glass bottom of the Petri dish has a grid of 500  $\mu$ m alphanumerically labeled squares which are used to determine the location of the interface in the hydrogel and the location of cells relative to that interface using microscopy.

#### 2.4 Hydrogel formation

After mixing all components of the precursor solution (including all gel components, particles and hMSCs) 34  $\mu L$  of precursor solution is injected into the PDMS ring of the sample chamber. To create an interface in stiffness, a photomask is used to spatially control UV light exposure. The photomask is a small square transparency ( $\approx 1~{\rm cm}\times 1~{\rm cm})$  with one half printed black with a resolution of 40 000 dots per inch (PhotomaskPORTAL). The transparency is placed on the PDMS ring in the sample chamber, covering half of the polymer precursor solution. The photomask is aligned with the grid in the bottom of the sample chamber using an alignment attachment. This attachment is 3D printed to fit over the PDMS ring, providing a straight edge that the photomask is aligned against. Details of this set-up are provided in our previously published work.  $^{36}$ 

To identify the exact location of the interface, which is the location where light starts to be attenuated by the photomask, we use an inverted microscope (Zeiss Observer Z1, Carl Zeiss AG) and a  $10\times$  objective (EC Plan-Neofluar, N.A. 0.3). Using the labels etched on the bottom of the Petri dish, the position where the photomask attenuates light is recorded. These markings are then referenced during data collection to determine where the cell being characterized is located in relation to the interface.

After noting the location of the change in UV light exposure, the sample chamber is placed under a light emitting diode (LED) UV lamp (M365LP1-C1, Thor Labs Inc.) which is collimated to a 10 mm diameter beam using a custom-made 3D printed collimator attachment.<sup>36</sup> This beam size matches the size of the PDMS ring in the sample chamber. Prior to exposing the hydrogel precursor, UV light intensity is set to 1.5 mW cm<sup>-2</sup> using a UV radiometer and LED driver (LEDD1B, Thor Labs Inc.).

The hydrogel is exposed to UV light for a total of 300 s. The photomask is removed after 270 s to expose the initially covered half for 30 s. We refer to this as a 300/30 s hydrogel. Our previous work verified that this set of UV exposure times for this hydrogel composition produces one half which is  $\approx 900$  Pa and the other half is  $\approx 300$  Pa, with a rapid change in elastic modulus of 600 Pa over an interface that is approximately 500  $\mu m$  thick.  $^{36}$  Representative data of the stiffness profile from 3 separate gels formed using this procedure is shown in the ESI† in Fig. S1.

Immediately after exposing the hydrogel, the sample chamber is filled with 4 mL of cell growth media without hFGF. The samples are then placed in an incubator (Galaxy 48R, Eppendorf) overnight at 37  $^{\circ}$ C and 5% CO<sub>2</sub> prior to microrheological data collection.

#### 2.5 Multiple particle tracking microrheology

hMSC remodeling of the pericellular region is measured using multiple particle tracking microrheology (MPT). MPT measures the Brownian motion of probe particles embedded in a sample to characterize changes in material structure and rheology. 33,39-42,48,49 Particle motion is captured using video microscopy and the trajectory of each particle is tracked using classical tracking algorithms.<sup>33,39,50</sup> Material rheology is related to particle motion, quantified by the ensemble-averaged mean-squared displacement (MSD,  $\langle \Delta r^2(\tau) \rangle$  where  $\tau$  is the lag time), using the Generalized Stokes-Einstein Relation (GSER). 10,39,41,42,48,49 The GSER can only be used to calculate moduli when certain conditions are met, including that the material is homogeneous, probe particles are moving due to only thermal motion and the native length scale of the material is much smaller than the probe particle. These calculations also require transformation of the data from the time to frequency domain, requiring truncation. 10,39,49 In our experiments, assumptions required to use the GSER are violated, therefore, we use the logarithmic slope of the MSD,  $\alpha$ .

α quantifies changes in material structure and cross-linking during cellular remodeling. A graphical representation of how  $\alpha$ is calculated is provided in the ESI† (Fig. S2).  $\alpha$  quantifies the state of the material using the shortest lag times (0.033-1 s). The shortest lag times are used because this data has the greatest number of particle displacements.  $\alpha$  values vary between 0 (indicating a gel) and 1 (indicating a fluid). When  $0 < \alpha < 1$ the material is a viscoelastic solid or fluid. When  $\alpha = n$ , where n is the critical relaxation exponent, the material transitions from a gel to a sol during degradation. n is calculated by analyzing degradation data using time-cure superposition. 10,39,51 From several previous studies, we have identified the value of n for our material.  $n = 0.25 \pm 0.05$  and is a material property. <sup>8,10,52</sup> n is independent of degree of cross-linking and is therefore the same across our hydrogel regardless of the stiffness in any particular region. $^{13,51,53}$  The value of n will only change when the structure of the material is changed, which can be done by changing the size of the components of the gel or changing the chemistry of the cross-linking reaction. 13,51,53

MPT data are collected using an inverted microscope (Zeiss Observer Z1, Carl Zeiss AG) and 63× water immersion objective (N.A. 1.3,  $1 \times$  optovar, Carl Zeiss AG). The microscope is equipped with an incubation chamber that maintains a 37 °C and 5% CO2 environment to ensure cell viability throughout the experiment. After locating a cell in the hydrogel, it is positioned roughly in the middle of the field of view and a brightfield image is taken to record its location. Immediately after taking the brightfield image, an 800 frame ( $\approx$  30 s) video of particle motion is taken at 30 frame s<sup>-1</sup> and exposure time of 1000 μs using fluorescence microscopy and a high speed camera (1024  $\times$  1024 pixels, approximately 160  $\mu$ m  $\times$  160  $\mu$ m, Miro M120, Vision Research Inc.). These camera settings are chosen to minimize static and dynamic error in the measurement.54 This procedure is repeated every 4-6 min for up to an hour or until the cell is no longer visible in the field of view. The stage is not moved throughout data collection. After characterizing a pericellular region, the location of the cell

is recorded by focusing on the grid on the base of the sample chamber. Data are collected on days 1, 2 and 6 postencapsulation to characterize both short- and long-time changes in pericellular rheology.

#### 2.6 Data analysis and statistics

Data are collected around a total of 90 cells, 30 hMSCs each on day 1, 2 and 6 post-encapsulation. Data are collected over the course of three separate experiments. Each experiment uses a different biological replicate and two different hydrogels are made per replicate (10 cells per biological replicate per postencapsulation day). Because cells are found prior to noting their location in the hydrogel, the distribution of locations of pericellular regions (in regions that are soft, stiff or in the interface) characterized in the material are not controlled. The number of cells whose pericellular regions are analyzed in each region of the hydrogel on each day post-encapsulation is shown in the ESI† in Fig. S3.

In this work we also analyze cell motility and shape. To calculate the speed of migrating cells, the center of mass of each cell is quantified using a program written in MATLAB (R2020a). The outer edge of the cell is traced and the center of mass of the cell is estimated as the average of all the points on the trace. This is repeated for each brightfield image collected through time of a single cell. Cell speed is calculated from each cell position between each video using

$$v_{\text{step}} = \frac{\sqrt{(x_{i+1} - x_i)^2 + (y_{i+1} - y_i)^2}}{t_{i+1} - t_i}.$$
 (1)

where  $v_{\text{step}}$  is the velocity of the cell between two time points,  $(x_{i+1},y_{i+1})$  is the position of the cell at time  $t_{i+1}$  and  $(x_i,y_i)$  is the position of the cell at time  $t_i$ . The initial cell location is i = 0 at t = 0 min, which is the time the cell is identified and data collection begins. Average cell velocity is calculated by averaging all  $v_{\text{step}}$  values for that cell.

The elliptical form factor (EFF) is calculated from the trace of the outline of the cell using a program in MATLAB (R2020a). This program creates a binary image from the trace of the cell and analyzes the shape. The covariance matrix of the binary image is calculated. The eigenvalues of this covariance matrix are the lengths of the major and minor axis of the ellipse which bounds the image. The length of the major and minor axis of the ellipse whose normalized second central moments are the same as the traced region are calculated and their ratio is the EFF.

Prior to conducting pairwise statistical testing, single factor analysis of variance (ANOVA, significance level of 0.01) is used to analyze the data in Fig. 2 and 3, grouped by the location relative to the interface. These tests indicate that significant differences exist between the tested populations. We then conduct pairwise statistical testing using a two-sample, unequal variance, heteroscedastic t-test. A difference between two measurements is considered statistically significant if p < 10.01. This level of significance is used because of the large number of samples analyzed in this work (748). Statistical testing is only conducted in regions where at least 3 different Soft Matter

measurements are taken and at least 2 cells are found. We do this because the t-test requires at least 3 points for each of the two populations and regions with one or fewer cells are not representative.

Probability density in Fig. 4 is calculated using a kernel smoothing function in MATLAB.

### 3 Results and discussion

In this work, we characterize the spatio-temporal evolution of the pericellular region around migrating hMSCs in a polymerpeptide hydrogel with a step-change or interface in stiffness. This material is composed of poly(ethylene glycol)-norbornene cross-linked with a peptide that is degradable by cell-secreted MMPs, making it easily remodeled by encapsulated cells. We create an interface between two halves of differing stiffness by spatially varying UV light exposure time during photopolymerization. To analyze how cellular remodeling varies with respect to position relative to this interface, we divide our hydrogel into 500 µm wide sections oriented parallel to the interface. These divisions are slightly larger than the distance a cell can feel, which is on the order of a few hundred microns. 9 The interface is a 500  $\mu$ m wide section where the elastic modulus, G', changes rapidly ( $\approx 1000 \text{ Pa mm}^{-1}$ ) between the two halves of different stiffness. 36 Since the stiffness profile of our hydrogel consists of two relatively uniform halves ( $G' \approx 900$  and 300 Pa) joined by a region of rapid increase in G', cells far from the interface are unaffected by the change in stiffness and behave similar to cells encapsulated in uniform hydrogels. Due to this, we characterize cell-mediated remodeling and degradation around cells that are in the soft or stiff region far from the interface and cells that are in the interface. We use multiple particle tracking microrheology (MPT) to measure changes in the rheology around each migrating cell and brightfield microscopy to measure cell speed and morphology. First, we analyze several parameters in different regions of the hydrogel: temporal pericellular rheology, cellular morphology, speed and persistence (the tendency of a cell to migrate in a single direction). We also measure spatial variations in pericellular rheology around single hMSCs. We measure that cells more easily remodel the soft half of the hydrogel in the first 2 days post-encapsulation and after 6 days, remodeling is similar everywhere. This shows that cell-mediated degradation is a function of initial cross-link density, with lower density regions being remodeled more easily than higher density regions. Additionally, cells migrate persistently towards stiff material and material rheology varies along the change in stiffness in the interface region.

We begin by measuring the logarithmic slope of the MSD,  $\alpha$ , for pericellular regions around cells 3D encapsulated in different sides of the interface and in the interface region on days 1, 2 and 6 post-encapsulation. The results of these measurements are shown in Fig. 1. t = 0 min is when the cell is initially located in the hydrogel on that day post-encapsulation. Each line in Fig. 1 is a representative pericellular region around an individual cell. These data are selected by graphing data for all cells in each

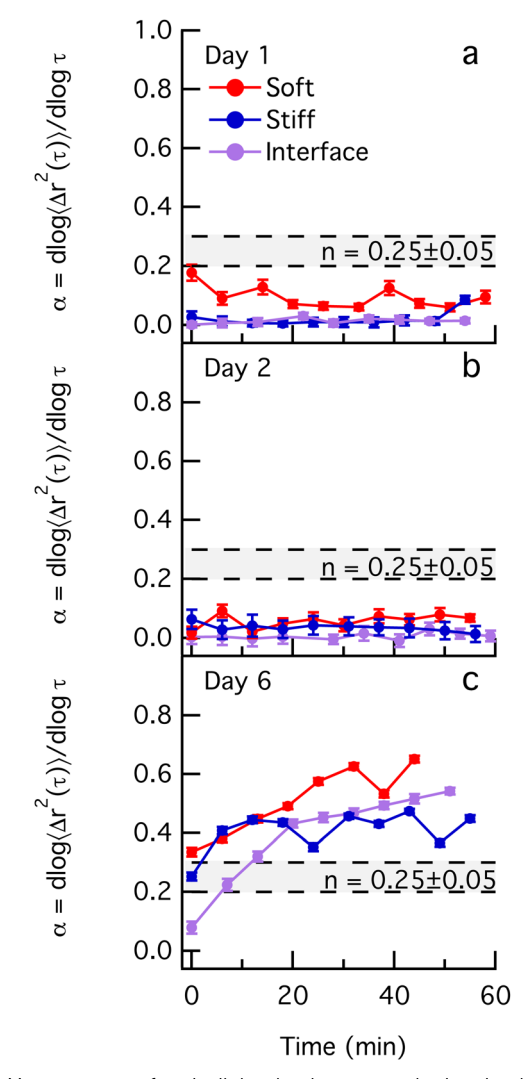


Fig. 1 Measurement of pericellular rheology around migrating hMSCs in each region of the hydrogel on days (a) 1, (b) 2 and (c) 6 post-encapsulation. The shaded area is the phase transition region when  $n=0.25\pm0.05$ , which is previously determined using time-cure superposition.  $^{8,10,52}$  Each curve shows representative data for the change in  $\alpha$  values around a different cell and each point on the curve is an individual MPT measurement of the entire field of view. Error bars represent the error in the slope when fitting a line to the MSD versus lag time,  $\tau$ .

region of the hydrogel (soft, stiff or in the interface) on each day post-encapsulation and selecting one which is representative of the entire data set. In each point of Fig. 1, the displacements of all particles are averaged together into a single MSD and  $\alpha$  is fit to this ensemble-averaged data.

On day 1 post-encapsulation (Fig. 1a), we measure relatively low  $\alpha$  values around cells in the soft, stiff and interface regions. All  $\alpha$  values are below the gel-sol transition region, the shaded region in Fig. 1, indicating that material in the pericellular region remains a gel. We do measure slightly higher α values around the cell in the soft half of the hydrogel. This is likely due to the lower initial cross-link density around this cell enabling the cell to degrade some cross-links in the network using cellsecreted MMPs resulting in higher particle mobility. The cells

**Paper** Soft Matter

in the interface region and stiff half of the hydrogel have not remodeled their surroundings and  $\alpha$  values remain close to 0. This is due to higher cross-link densities in these regions requiring more time for cells to degrade the material and particle mobility to increase.

Day 2 post-encapsulation (Fig. 1b) has similar trends to day 1. The material around each cell remains in the gel state as cellsecreted MMPs have not had sufficient time to break cross-links within the material.

By day 6 post-encapsulation (Fig. 1c), significant degradation has occurred in all regions of the hydrogel. This is measured by increased values of  $\alpha$  past the gel-sol transition around each cell regardless of its location in the hydrogel. We measure that  $\alpha$ values for material around the cell in the soft side of the hydrogel begin as a sol and the  $\alpha$  value increases, indicating more crosslinks are broken. It should be noted that the starting point for each curve is arbitrary since data collection begins when we locate the cell in the hydrogel meaning the starting  $\alpha$  value is not representative of the starting material properties.  $\alpha$  values likely increase more for material around the cell in the soft half due to the lower initial cross-link density. The material around the cell in the stiff side of the hydrogel initially begins with an  $\alpha$  value in the phase transition region and the value of  $\alpha$  remains relatively constant after its surroundings are degraded into the sol state. The final value of  $\alpha$  is lower than the value measured in the soft side of the hydrogel, indicating that there is lower probe particle mobility due to remaining cross-links between polymers. The smaller change in  $\alpha$  values for the material around this cell is likely due to the higher initial cross-link density in this half of the hydrogel requiring cells to secrete more MMPs to degrade the material. Previous microrheological characterization of these hydrogels showed that the rate of change of  $\alpha$  with time is slower for gels with higher initial G' and their  $\alpha$  values tend to be lower than the  $\alpha$  values for softer hydrogels at the same time postencapsulation.<sup>13</sup> The rheology of the material in the interface region is similar to the material in the soft region, degrading to a sol as MMPs break cross-links in the network.

Fig. 1 provides a measurement of the temporal evolution of the entire pericellular region around different cells in different stiffness environments. This data only provides information about material around an individual cell. In order to quantify how cells in each region of the hydrogel degrade their pericellular region, we plot the average  $\alpha$  value,  $\alpha_{avg}\text{,}$  measured in different 500 μm wide sections oriented parallel to the interface on each day in Fig. 2.

On day 1 post-encapsulation (Fig. 2a), we measure relatively low degradation in each section of the hydrogel. Most regions have  $\alpha_{avg}$  values that are below the phase transition region, indicating that the material remains a gel. This agrees with data for single pericellular regions in Fig. 1a. We measure a statistically significant increase in the value of  $\alpha_{avg}$  at 1.5–2.0 mm from the interface in the soft half of the hydrogel relative to all other distances. It should be noted that the 2.0-2.5 mm region in the soft side is not tested against any other region for statistical significance since only one cell is measured in this region. This increase in the value of  $\alpha_{avg}$  1.5–2.0 mm from the

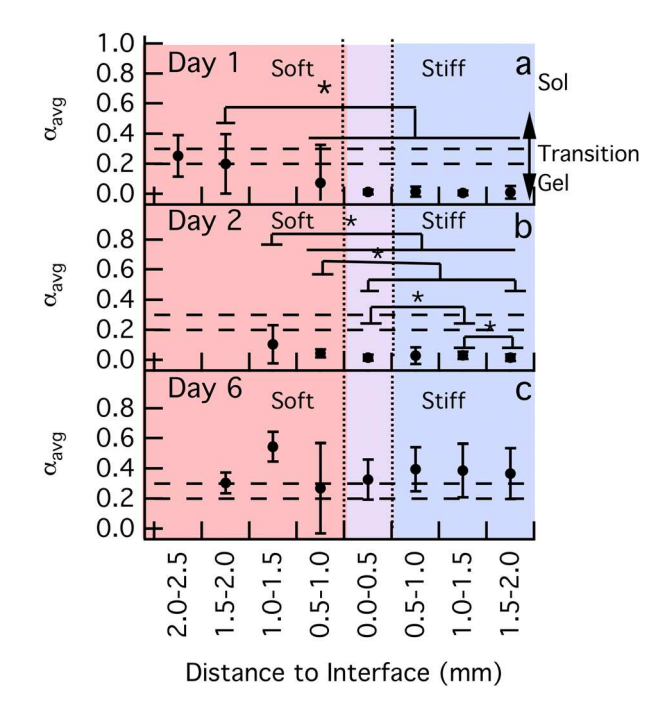


Fig. 2 Average  $\alpha$  values,  $\alpha_{\text{avg}}$  in the pericellular region as a function of position relative to the interface on days (a) 1, (b) 2 and (c) 6 postencapsulation. Data are  $\alpha_{\text{avg}}$  values for all measurements in that section with error bars equal to the standard deviation. The background colors represent the different regions of the hydrogel. The soft and stiff halves are represented by red and blue, respectively, and purple represents the region of rapid change in G' in the interface.\*: p < 0.01.

interface in the soft half of the hydrogel is due to the reduced initial cross-link density surrounding these cells. Cells in regions closer to the interface (0.5-1.0 mm in the soft side, the interface region and the stiff half of the hydrogel) are able to feel changes in stiffness and may remodel more significantly in response. Previous work has shown these MMP secretions increase in response to an increase in stiffness felt by cells.<sup>35</sup>

On day 2 post-encapsulation (Fig. 2b), we measure small but significant differences in  $\alpha_{avg}$  between the soft and stiff regions of the hydrogel.  $\alpha_{avg}$  at 1.0-1.5 mm in the soft half of the hydrogel is higher than all other measured locations. Additionally,  $\alpha_{\rm avg}$  for 0.5–1.0 mm in the soft half is higher than the interface region and 1.5-2.0 mm from the interface in the stiff half. These differences are the result of the reduced cross-link density on the soft side of the hydrogel leading to more rapid degradation of the scaffold by cell-secreted MMPs. While there are other statistically significant differences between regions in the hydrogel, most material remains a gel with  $\alpha_{avg} < n$ . The higher  $\alpha_{avg}$  values in the soft half of the hydrogel on day 1 postencapsulation are measured far from the interface, more than 1.5 mm away. The pericellular regions characterized in the soft half of the hydrogel on day 2 post-encapsulation are all close to the interface (within 1.5 mm) and have similar  $\alpha_{avg}$  to those measured on day 1 post-encapsulation at 0.5-1.0 mm from the interface in the soft side. We hypothesize that if cells further from the interface in the soft half of the hydrogel are characterized on day 2 post-encapsulation, they will have higher  $\alpha_{avg}$ 

values, since  $\alpha_{avg}$  values will increase with time as cross-links are irreversibly degraded.

On day 6 post-encapsulation (Fig. 2c) we measure large increases in  $\alpha_{avg}$  in all regions of the hydrogel relative to previous days. Most regions transition from a gel to a sol. Additionally,  $\alpha_{avg}$  is relatively constant throughout the hydrogel, indicating that cross-link density is similar everywhere in the hydrogel regardless of the starting material modulus. Results by Daviran et al. show that for the same hydrogel formulation with uniform initial cross-link density,  $\approx 80\%$  of cells encapsulated in a gel with  $G' \approx 300$  Pa (the stiffness of the soft half of our hydrogel) have remodeled their surroundings by day 6 postencapsulation.<sup>13</sup> Only a small reduction in this percentage (5% reduction to 75%) is measured when G' is increased to  $\approx 900$  Pa (the stiffness of the stiff half of our hydrogel). Additionally, Mazzeo et al. measured that the same hydrogel is nearly completely degraded by the same concentration of encapsulated hMSCs after 72 hours using bulk rheology. From these previous findings and our measurement of  $\alpha_{avg}$  in each position, we hypothesize that the differences in stiffness between each half of the hydrogel and the interface region is significantly reduced from cellular remodeling. It might be expected that the soft half of the hydrogel will degrade before the stiff half and will always have higher  $\alpha_{avg}$  values until complete degradation. However, MMP activity is increased when hMSCs are encapsulated in materials of higher cross-link density.35 This could cause the cells in the stiff half of the hydrogel to secrete more MMPs and fewer inhibitors of MMPS (specifically tissue inhibitors of metalloproteinases, TIMPs) than cells in the soft half of the gel. This change in secretion of MMPs and TIMPs, we hypothesize, could result in similar amounts of degradation everywhere in the hydrogel 6 days postencapsulation, which is measured in Fig. 2c.

Material stiffness has also been shown to change cell morphology, which affects cell motility. Previous work has shown that cells encapsulated in soft materials are able to spread easily as they modify their surrounding structure resulting in extended morphologies. 15,55 We quantify cell morphology by measuring the elliptical form factor (EFF) of our cells, which is the ratio of the major axis length to the minor axis length of the ellipse whose normalized second central moment is the same as the traced cell area. EFF for a perfect circle is equal to 1. Cells with extended morphologies will have higher EFF. Measuring cell shape is complex and, in this work, we describe cell shape using a single parameter, EFF. We do recognize that there are many methods to describe cell shape and that the EFF describes only a single aspect of this complex parameter.56,57 Although this is a single representative value, it is a quantitative measure that captures key aspects of cell shape and we have provided visualizations of cell traces and their major and minor axes in the ESI† (Fig. S4). The results of the measurement of EFF are in Fig. 3.

On day 1 post-encapsulation (Fig. 3a), we measure statistically different values of EFF across the hydrogel due to the different microenvironmental stiffnesses experienced by cells in each region. We measure the highest EFF in the interface region. Cells in the interface region are likely extending in response to

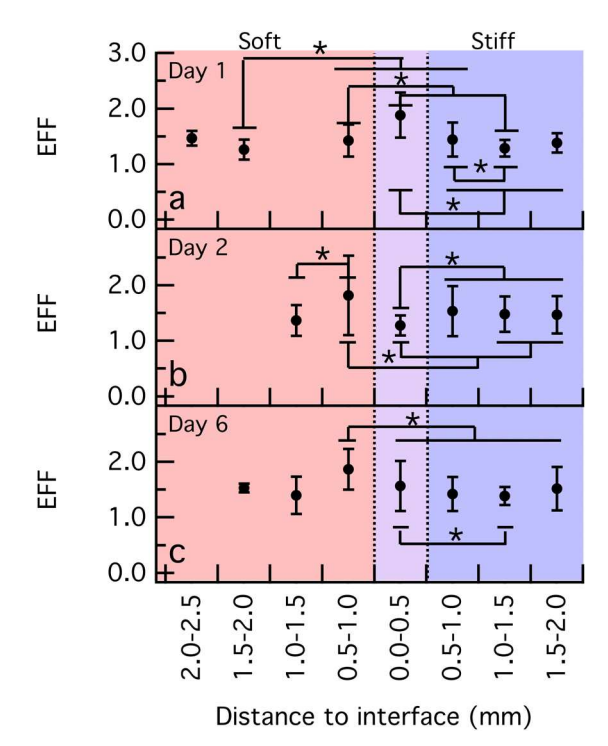


Fig. 3 EFF as a function of position relative to the interface on days (a) 1, (b) 2 and (c) 6 post-encapsulation. The background color in each graph represents the region of the hydrogel being measured: red represents the soft half, blue represents the stiff half and purple represents the interface region.\*: p < 0.01.

the rapid change in stiffness, increasing their EFF. These cells are also aligning their displacements with the gradient in G'present in this region indicating that the physical cue provided by the interface is affecting both cell displacements and morphology. Alignment of cell displacements is discussed in detail below. Other than cells in the interface region, EFF tends to be lowest on day 1 post-encapsulation since cells have not been able to remodel their pericellular regions and stretch.

On day 2 post-encapsulation (Fig. 3b), the highest value of EFF is 0.5-1.0 mm from the interface in the soft side of the hydrogel. This point also has a high standard deviation, indicating that cells in this region have variable morphologies. This is likely due to varied amounts of degradation in this region, which create distinct microenvironments that significantly change cell spreading. The EFF for cells 0.5-1.0 mm from the interface in the soft side is statistically higher than the EFF for cells 1.0-1.5 mm from the interface in the soft side and 1.0-2.0 mm in the stiff side. Cells in these regions far from the interface can not sense the change in stiffness in the interface and do not change their morphology. EFF is lowest in the interface region, possibly because the cells characterized on day 2 are located closer to the stiff half of the hydrogel and are not able to extend effectively into material which is not significantly degraded. On average, EFF increases in the soft and stiff regions of the hydrogel relative to day 1 post-encapsulation. Additionally, on day 2 post-encapsulation, EFF for cells in the soft half is greater than or equal to EFF for cells in the stiff half.

Paper

As cells remodel their surroundings, they are able to extend more, increasing their EFF.

On day 6 post-encapsulation (Fig. 3c), EFF increases relative to previous days since cells have degraded their surroundings and are able to spread and migrate. The highest value of EFF continues to be at 0.5-1.0 mm from the interface in the soft side of the hydrogel. We measure that cells in this region are significantly more spread than those in the stiff half of the hydrogel, but that the spreading is not significantly different from other cells in the soft half. The difference between the interface region and the soft region is not statistically significant.

Fig. 2 shows measurements of the state of the material in each region of the hydrogel. We measure that the hydrogel is degraded by hMSCs differently based on the initial cross-link density, but that these differences are not significant by day 6 post-encapsulation. hMSCs degrade their surroundings so that they can extend into newly degraded space, attach and migrate. Fig. 3 shows changes in cell morphology in each region showing that in general cells in the soft half of the hydrogel are more extended. Since degradation and morphology have both previously been shown to change cell migration, we quantify cell speed in each region of the hydrogel. 10,55,58 On each day postencapsulation, we measure similar cell speeds in each region with an average speed of approximately 10-40 μm h<sup>-1</sup>. These results are provided in the ESI† in Fig. S5. Although no difference in cell speed is measured, we further analyze motility. We measure the tendency of the cell to migrate in the same direction, called cell persistence, in each region of the hydrogel in Fig. 4.

Persistence of hMSC motility is quantified by measuring the orientation of cell displacements relative to the stiffness gradient in the interface. Persistent cell migration towards stiff material is called durotaxis and is an example of cells responding to a physical cue provided by their surroundings.<sup>59,60</sup> To determine if cells in different regions of the hydrogel are responding to the change in stiffness by changing their motility, we measure the sine of the angle of the net cell displacement,  $\sin \theta$ , relative to the interface. Values of  $\sin \theta$  close to 1 indicate that the cell is persistently migrating towards the stiff half of the hydrogel. Conversely, values of  $\sin \theta$  close to -1 indicate that the cell is persistently migrating towards the soft half of the hydrogel. We take the first and last cell locations for each cell characterized in the hydrogel and calculate the net x and y displacement. Then we use those displacements to calculate  $\sin\theta$  for each cell. We compute a probability distribution function (PDF) of  $\sin \theta$  to show the distribution of the data. These PDFs are plotted in Fig. 4. Only regions with at least 3 measurements are used to calculate PDFs to prevent misinterpretation of regions with a small number of cells. Regions of high probability are green and blue and regions of low probability are white and brown. Peaks in probability show that most cells in that region are migrating with that  $\sin \theta$ . These are visualized by thin blue and green bars in Fig. 4.

On day 1 post-encapsulation (Fig. 4a), in most areas of the hydrogel we don't measure significant alignment of hMSC displacements relative to the interface. This is shown by

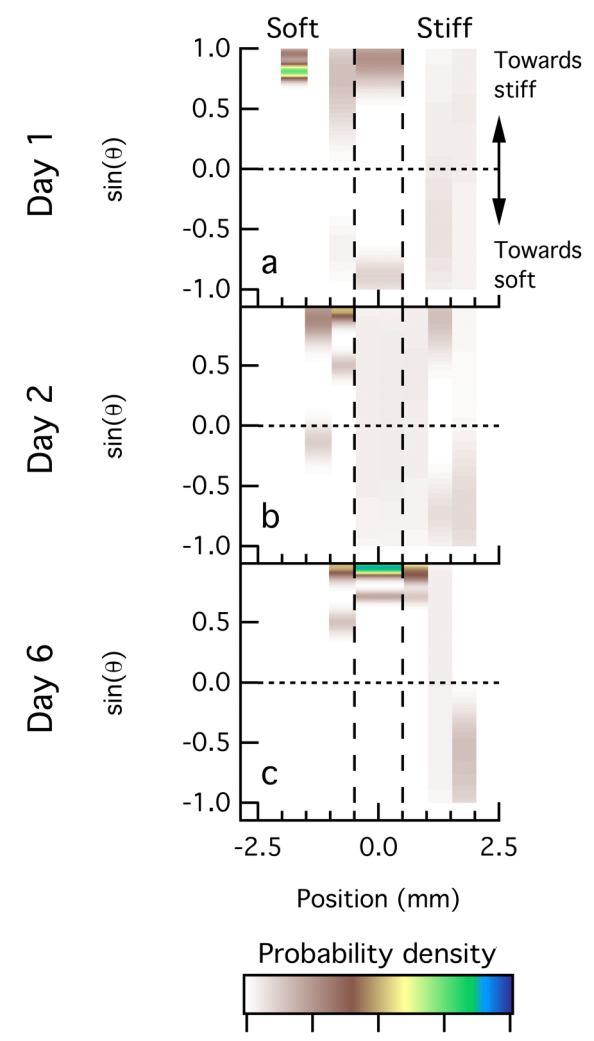


Fig. 4 Probability distribution functions (PDFs) of the alignment of cell displacements, quantified as  $\sin \theta$  where  $\theta$  is measured with respect to the interface, on days (a) 1, (b) 2 and (c) 6 post-encapsulation. Values of  $\sin \theta$ close to 1 indicate the cell is migrating in the direction of the stiff half of the hydrogel. Values of  $\sin \theta$  close to -1 indicate the cell is migrating in the direction of the soft half of the hydrogel. Probability is represented by color with white and brown indicating low probability and yellow, green and blue indicating high probability. The horizontal dotted line indicates where cells do not migrate towards either half of the hydrogel,  $\sin \theta = 0$ . The vertical dashed lines represent the interface region.

2

6

0

probability distributions with no significant peaks (mostly brown and white in the Fig. 4a). This is likely due to little cell-mediated degradation this early post-encapsulation limiting the amount of migrating cells. The only region where some alignment occurs is 1.5-2.0 mm from the interface in the soft side of the hydrogel. This region has  $\sin \theta \approx 0.8$  which equates to an angle of approximately 53° with the horizontal formed by the interface. This region has been degraded to the gel-sol transition in Fig. 2a. Additionally, cells in this region are near the edge of the hydrogel and are preferentially migrating deeper into the hydrogel, possibly following the durotactic cue to migrate towards the stiffer material and away from the fluid

environment outside of the gel scaffold. If hMSCs did migrate to the edge, they could leave the hydrogel and enter the media, which is a fluid and not a preferred environment for hMSCs. These factors can cause cells to migrate more persistently towards stiffer material.

On day 2 post-encapsulation (Fig. 4b), we again do not measure significant alignment. For example, the PDF in the interface region is a uniform light brown color, indicating that cells migrate with equal probability in all directions.  $\alpha$  values remain low on this day post-encapsulation indicating cells have not significantly remodeled their surroundings, shown in Fig. 2b, and are therefore not able to migrate persistently or align themselves in any direction.

On day 6 post-encapsulation we measure alignment of hMSC displacements towards stiff regions of the hydrogel. The PDF peaks at  $\sin \theta \approx 0.9$  in the interface region and 0.5-1.0 mm from the interface in the stiff side. This corresponds to an angle of  $\approx 26^{\circ}$  with the vertical, indicating that the net migration of cells in this region is in the direction of the stiff half of the hydrogel. The alignment of cell displacements in the interface region and 0.5-1.0 mm from the interface in the stiff side of the hydrogel on day 6 post-encapsulation is likely due to durotaxis. In other regions of the hydrogel, cells are migrating randomly with no alignment. This directed migration is unique to the interface region on day 6. Regions other than the interface do not have directed cell displacements because these areas are uniform and lack durotactic cues.

Cell migration and material remodeling create unique spatio-temporal degradation profiles in the pericellular region, which we characterize using MPT. Previous work in uniform hydrogels has shown that cells secrete MMPs resulting in a radial pattern of degradation. hMSCs secrete both MMPs and their inhibitors, TIMPs, to create microenvironments that enable stretching, attachment and motility.8,12,61,62 Because our hydrogel is composed of two relatively uniform stiffness halves separated by a region of rapid change in stiffness in the interface, we hypothesize that cells far from the interface will have degradation profiles which vary radially. Therefore, we map the rheology of the pericellular region by calculating  $\alpha$ values in the soft and stiff halves spatially by splitting the field of view into a series of colored rings centered at the cell center. The results for spatial variation in hMSC remodeling in uniform stiffnesses are the left and right columns in Fig. 5-7. The graphs are oriented so that the positive *y*-direction is towards the stiff half of the hydrogel and the negative y-direction is towards the soft half. Each graph has a brightfield image of the cell and its pericellular region in the background. Superimposed onto the image are a series of colored regions. The rings are R = R150 pixels (23.4  $\mu$ m) wide centered around the cell center. Only the particle displacements in each ring are used to calculate the  $\alpha$ value, which is represented by the color of the ring. Each ring is sized to ensure that enough particles are present for accurate microrheology measurements, which is approximately 10-50 particles per ring.

Cells in the interface are able to sense the rapid change in G'. For this region, we split the field of view into 40 µm wide

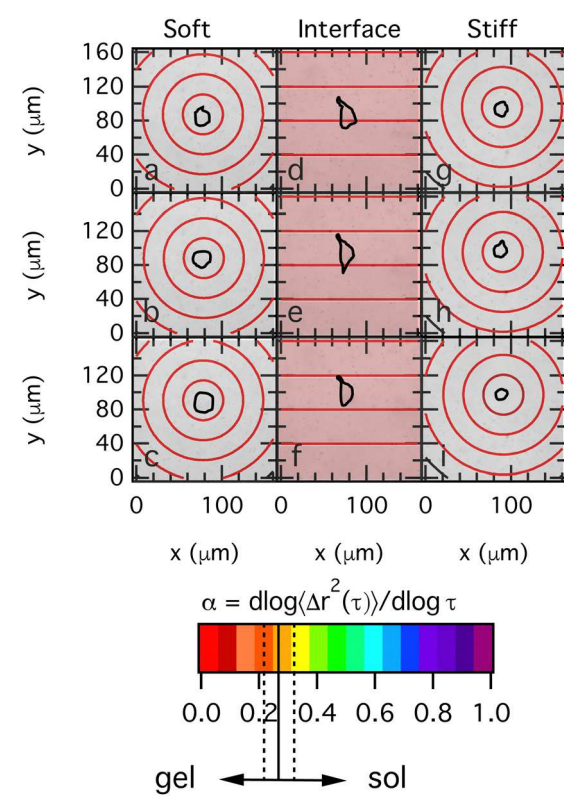
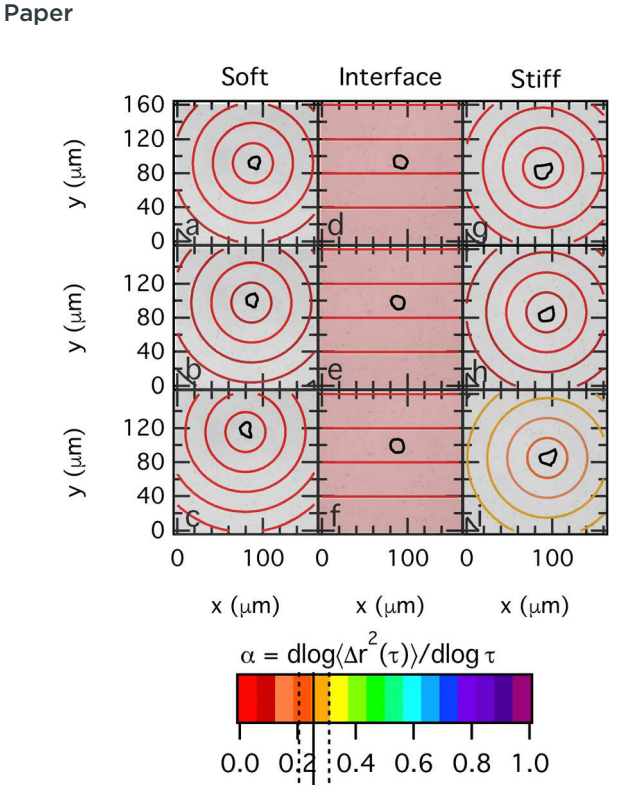


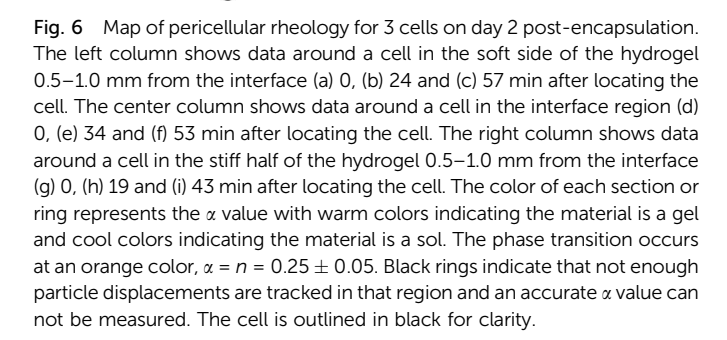
Fig. 5 Map of pericellular rheology for 3 cells on day 1 postencapsulation. The left column are data around a cell in the soft side of the hydrogel 0.5-1.0 mm from the interface (a) 0, (b) 31 and (c) 57 min after locating the cell. The center column are data around a cell in the interface region (d) 0, (e) 37 and (f) 56 min after locating the cell. The right column shows data around a cell in the stiff half of the hydrogel 0.5–1.0 mm from the interface (g) 0, (h) 30 and (i) 61 min after locating the cell. The color of each section or ring represents the  $\alpha$  value with warm colors indicating the material is a gel and cool colors indicating the material is a sol. The phase transition occurs at an orange color,  $\alpha = n = 0.25 \pm 0.05$ . Black rings indicate that not enough particle displacements are measured in that region for good statistics and an accurate  $\alpha$  value can not be calculated. The cell is outlined in black for clarity.

sections oriented parallel to the interface. The width of these sections is chosen to ensure enough particles are present for accurate MPT measurements. We divide the field of view in this way to characterize a region with a small change in G' that is the same length scale as a hMSC. Additionally, cells may orient their remodeling in a gradient with the interface, with more remodeling closer to one half of the hydrogel than another. This would not be quantitatively captured if we used a series of rings as we do for the cells in the uniform regions.

Fig. 5 shows one cell randomly selected from each region of the hydrogel. On day 1 post-encapsulation,  $\alpha$  values remain low indicating minimal degradation. All material in the pericellular region remains a gel. This is likely because cells have not had enough time to remodel their microenvironments. There are no significant differences in pericellular degradation in the three regions measured in Fig. 5.

On day 2 post-encapsulation (Fig. 6), material in all regions of the field of view of the cells remain a gel and little





sol

gel

degradation is measured. This is similar to the results shown in Fig. 2b where the  $\alpha$  values remain low throughout the hydrogel. A change in pericellular rheology is measured around the cell in the stiff half of the hydrogel (Fig. 6g-i). The cell in the stiff half remodels its material into the transition region 43 min after being located (Fig. 6i). This cell is actively remodeling its surroundings and has a higher  $\alpha$  value than the cell in the soft half. In Fig. 6i, the  $\alpha$  value of each ring increases with distance from the cell center, indicating more degradation further from the cell than immediately around it, a reverse reaction-diffusion profile. This degradation profile is due to the secretion of both MMPs and TIMPs by the hMSC.8,11,61,62 When MMPs are secreted, they are quickly bound by cell-secreted TIMPs, preventing their activity. The MMP-TIMP complex diffuses away from the cell and unbinds enabling MMPs to start breaking crosslinks resulting in degradation far from the cell.<sup>8,61,62</sup>

On day 6 post-encapsulation (Fig. 7), more remodeling is measured than on previous days. By day 6, the cumulative effect of MMPs on the network has reduced the number of cross-links

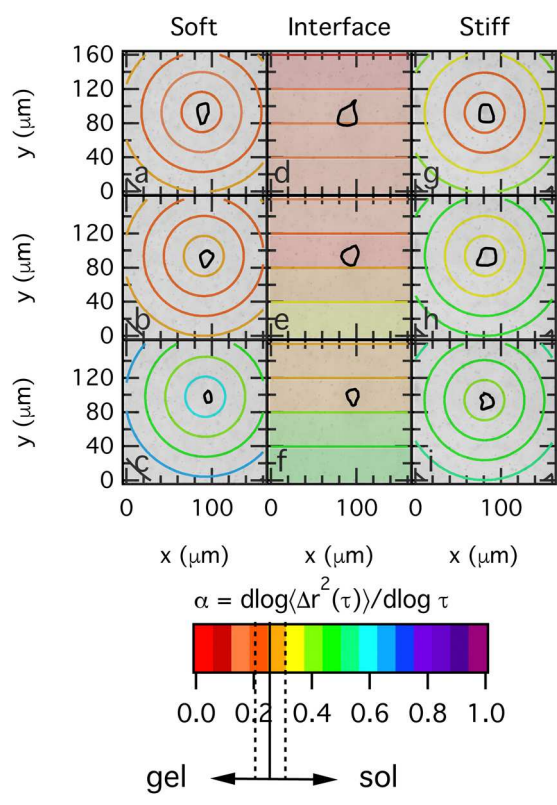


Fig. 7 Map of pericellular rheology for 3 cells on day 6 post-encapsulation. The left column shows data around a cell in the soft side of the hydrogel 0.5-1.0 mm from the interface (a) 0, (b) 12 and (c) 31 min after locating the cell. The center column shows data around a cell in the interface region (d) 0, (e) 31 and (f) 56 min after locating the cell. The right column shows data around a cell in the stiff half of the hydrogel 0.5-1.0 mm from the interface (g) 0, (h) 18 and (i) 36 min after locating the cell. The color of each section or ring represents the  $\alpha$  value with warm colors indicating the material is a gel and cool colors indicating the material is a sol. The phase transition occurs at an orange color  $\alpha = n = 0.25 \pm 0.05$ . Black rings indicate that not enough particle displacements are tracked in that region and an accurate  $\alpha$  value can not be measured. The cell is outlined in black for clarity

making particle motion measurable, increasing  $\alpha$ . Further degradation from cell-secreted MMPs causes  $\alpha$  to rapidly increase past the gel-sol transition, which is measured in Fig. 7. Additionally, many cells have settled out of the gel and on to the glass bottom of the Petri dish by day 6 postencapsulation. Therefore, the cells that are still 3D encapsulated are in regions that will undergo rapid cell-mediated degradation. The cell in the soft region of the hydrogel (Fig. 7a-c) has  $\alpha \approx 0.25$  for all regions at t=0 min and t=012 min (Fig. 7a and b, respectively) indicating that the pericellular region is undergoing a phase transition. By 31 min (Fig. 7c) the material in the pericellular region is degraded from cell-secreted MMPs and has  $\alpha \approx 0.40$ –0.65. In Fig. 7a–c (the soft region), the highest  $\alpha$  value is far from the cell (93.6  $\mu$ m) and the second highest is immediately around the cell (23.4 µm) with intermediate  $\alpha$  values elsewhere. Previous work by Daviran *et al.* shows that 6 days post-encapsulation, cells in hydrogels with  $G' \approx 300$  Pa (the same modulus as the soft half of our hydrogel) have either completely degraded their surroundings or have a degradation

profile similar to those shown in Fig. 7a-c.<sup>13</sup> They show that this profile occurs when material is in or near the phase transition region, which is what we measure in Fig. 7a and b.<sup>13</sup>

Soft Matter

More degradation is measured around the cell in the interface (Fig. 7d-f) towards the soft half of the hydrogel (decreasing y-direction) and less degradation towards the stiff half (positive y-direction). Additionally, the material in each horizontal section is more degraded with time and the cell is migrating in the positive y-direction towards regions of higher stiffness. We hypothesize that this gradient in degradation is because of the steep gradient in cross-link density present at the interface  $(dG'/dx \approx 1000 \text{ Pa mm}^{-1})$ . Cell-secreted MMPs degrade material closer to the soft half of the hydrogel easily because these regions have fewer cross-links. Regions closer to the stiff half of the hydrogel require more cross-links to be broken by MMPs to be degraded, resulting in lower  $\alpha$  values at higher y-coordinates. It may be expected that the degradation profile around the cell in the interface region would continue to be radially symmetric due to cell-mediated degradation, like those in the uniform regions of the hydrogel. We hypothesize that the change in material stiffness in the interface region has a more significant impact than the radial nature of cell secretions. This hypothesis is supported by the data where we measure material degradation is in the same direction as the gradient. If the profile continued to be radially symmetric, we would measure a symmetric pattern of values of  $\alpha$  around the cell in the ydirection. Instead, we measure a gradient in  $\alpha$  in the ydirection, indicating that material degradation is a function of the initial cross-link density in the interface region.

The cell in the stiff region (Fig. 7g–i) creates a different degradation profile in the pericellular region than the cell in the soft region. While degradation of the pericellular region increases with time, degradation also increases with increasing distance from the cell. Previous work has shown that the interaction between MMPs and TIMPs creates this reverse reaction–diffusion degradation profile. 8,61,62 Degradation is also faster in the soft half of the hydrogel than in the stiff half. The  $\alpha$  value increases more rapidly in each ring around the cell in the soft half of the hydrogel (from  $\alpha \approx 0.2$  to  $\alpha \approx 0.5$  in  $\approx 31$  min) than around the cell in the stiff half (from  $\alpha \approx 0.3$  to  $\alpha \approx 0.45$  in  $\approx 36$  min), likely due to the ease of degradation of the soft half because of the lower cross-link density.

The results in Fig. 5–7 indicate that cells in both the soft and stiff halves of the hydrogel have different degradation profiles, which change because of the stiffness of the surrounding material. Remodeling is determined by hMSC-secretion of MMPs and TIMPs regulating pericellular degradation. <sup>8,61</sup> We do conduct further analysis of the interface region, but because of the limited number of pericellular regions characterized, we can not draw major conclusions. We provide this analysis to highlight the methodology in the ESI.†

## 4 Conclusions

This work uses multiple particle tracking microrheology (MPT) to characterize changes in pericellular rheology around cells in

a hydrogel with an interface in elastic modulus. We measure that cells remodel their pericellular regions and tend to migrate towards stiff regions of the hydrogel. Cells in the soft region of the hydrogel are able to remodel their surroundings at earlier times post-encapsulation due to a lower initial cross-link density. On days 1 and 2 post-encapsulation, almost all remodeling is restricted to the soft half of the hydrogel. By day 6 postencapsulation, all regions of the gel (soft, interface and stiff) are remodeled due to cell-secreted MMPs breaking cross-links. We measure cell motility in response to the change in stiffness. Cells in the interface undergo durotaxis, orienting their migration towards the stiff region of the hydrogel on day 6 postencapsulation. On all days, cells in stiff regions and most cells in the soft regions of the hydrogel migrate randomly, have a uniform distribution of  $\sin \theta$  and are not directed. Finally, we measure changes in pericellular rheology in each half of the hydrogel and in the interface region. Cells in the uniform stiffness regions of the hydrogel on day 6 post-encapsulation have pericellular degradation profiles which vary radially and agree with previous results. Cells in the soft half have random degradation profiles and are degrading the material through the gel-sol phase transition while those in the stiff half have reverse reaction-diffusion profiles. On days 1 and 2 postencapsulation, the interface is not degraded. By day 6 postencapsulation, degradation varies in a gradient in the interface region with more degradation near the soft material and less degradation near the stiff material. Degradation and persistence are also related on day 6 post-encapsulation. The soft and stiff halves of the hydrogel have cells that migrate randomly since there is no direction in their remodeling while the cells in the interface migrate persistently towards the stiff material which has lower  $\alpha$  values.

The results presented in this work can be used to improve the design of implantable hydrogels for wound healing and cell delivery. We've shown that hMSC behavior is highly variable in regions of rapid changing G' similar to the microenvironments cells would experience when being delivered out of a hydrogel and into a wound. Our results show that cells remodel their surroundings to enable migration, suggesting that they will need to remodel the implant-tissue interface to leave the scaffold and participate in healing. These results show that more complex materials that contain regions of different stiffnesses have more diverse cellular microenvironments. These complex materials will better mimic aspects of native tissue, which will enable cells to have the desired morphology, migration and lineage specification to regenerate this tissue.

### **Author contributions**

J. A. M.: Data curation, formal analysis, investigation, methodology, project administration, validation, visualization, writing – original draft and writing – review and editing. K. M. S.: conceptualization, funding acquisition, project administration, resources, supervision and writing – review and editing.

# Conflicts of interest

There are no conflicts to declare.

# Acknowledgements

Funding for this work was provided by the National Science Foundation (NSF) under Grant No. CBET-1751057 and the John C. Chen Graduate Fellowship for partial support of JAM.

# Notes and references

- 1 M. Otero-Viñas and V. Falanga, Adv. Wound Care, 2016,
- 2 E. Eggenhofer, F. Luk, M. H. Dahlke and M. J. Hoogduijn, Front. Immunol., 2014, 5, 148.
- 3 S. J. Morrison and D. T. Scadden, Nature, 2014, 505, 327.
- 4 W. J. Ennis, A. Sui and A. Bartholomew, Adv. Wound Care, 2013, 2, 369-378.
- 5 L. Shin and D. A. Peterson, Stem Cells Transl. Med., 2013, 2,
- 6 S. Maxson, E. A. Lopez, D. Yoo, A. Danilkovitch-Miagkova and M. A. LeRoux, Stem Cells Transl. Med., 2012, 1, 142-149.
- 7 A. J. Singer and R. A. Clark, N. Engl. J. Med., 1999, 341,
- 8 M. Daviran, S. M. Longwill, J. F. Casella and K. M. Schultz, Soft Matter, 2018, 14, 3078-3089.
- 9 M. S. Rudnicki, H. A. Cirka, M. Aghvami, E. A. Sander, Q. Wen and K. L. Billiar, Biophys. J., 2013, 105, 11-20.
- 10 J. A. McGlynn, K. J. Druggan, K. J. Croland and K. M. Schultz, Acta Biomater., 2020, 405-417.
- 11 H. Nagase, R. Visse and G. Murphy, Cardiovasc. Res., 2006, 69, 562-573.
- 12 K. M. Schultz, K. A. Kyburz and K. S. Anseth, Proc. Natl. Acad. Sci. U. S. A., 2015, 112, E3757-E3764.
- 13 M. Daviran, J. Catalano and K. M. Schultz, Biomacromolecules, 2020, 21, 3056-3068.
- 14 J. A. McGlynn, K. J. Druggan, K. J. Croland and K. M. Schultz, Acta Biomater., 2021, 121, 405-417.
- 15 K. A. Kyburz and K. S. Anseth, Acta Biomater., 2013, 9, 6381-6392.
- 16 S. B. Anderson, C.-C. Lin, D. V. Kuntzler and K. S. Anseth, Biomaterials, 2011, 32, 3564-3574.
- 17 A. P. Dhand, J. H. Galarraga and J. A. Burdick, Trends Biotechnol., 2021, 39, 519-538.
- 18 C. Loebel, R. L. Mauck and J. A. Burdick, Nat. Mater., 2019, 1,883-891.
- 19 W. J. Hadden, J. L. Young, A. W. Holle, M. L. McFetridge, D. Y. Kim, P. Wijesinghe, H. Taylor-Weiner, J. H. Wen, A. R. Lee and K. Bieback, et al., Proc. Natl. Acad. Sci. U. S. A., 2017, 114, 5647-5652.
- 20 O. Chaudhuri, L. Gu, D. Klumpers, M. Darnell, S. A. Bencherif, J. C. Weaver, N. Huebsch, H.-P. Lee, E. Lippens and G. N. Duda, et al., Nat. Mater., 2016, 15, 326.
- 21 A. Singh and N. A. Peppas, Adv. Mater., 2014, 26, 6530-6541.

- 22 J. D. McCall, J. E. Luoma and K. S. Anseth, Drug Delivery Transl. Res., 2012, 2, 305-312.
- 23 A. J. Engler, S. Sen, H. L. Sweeney and D. E. Discher, Cell, 2006, 126, 677-689.
- 24 J. R. Tse and A. J. Engler, PLoS One, 2011, 6, e15978.
- 25 Y. Berkovitch and D. Seliktar, Int. J. Pharm., 2017, 523, 545-555.
- 26 C. D. Hoemann, C.-H. Lafantaisie-Favreau, V. Lascau-Coman, G. Chen and J. Guzmán-Morales, J. Knee Surgery, 2012, 25, 085-098.
- 27 M. Kar, Y.-R. V. Shih, D. O. Velez, P. Cabrales and S. Varghese, Biomaterials, 2016, 77, 186-197.
- 28 S. B. Anderson, C. Lin, D. V. Kuntzler and K. S. Anseth, Biomaterials, 2011, 32, 3564-3574.
- 29 D. D. McKinnon, D. W. Domaille, T. E. Brown, K. A. Kyburz, E. Kiyotake, J. N. Cha and K. S. Anseth, Soft Matter, 2014, 10, 9230-9236.
- 30 B. Yang, Y. Zhang, X. Zhang, L. Tao, S. Li and Y. Wei, Polym. Chem., 2012, 3, 3235-3238.
- 31 R. A. Marklein and J. A. Burdick, Soft Matter, 2010, 6, 136-143.
- 32 A. Seidi, M. Ramalingam, I. Elloumi-Hannachi, S. Ostrovidov and A. Khademhosseini, Acta Biomater., 2011, 7, 1441-1451.
- 33 J. A. McGlynn, N. Wu and K. M. Schultz, J. Appl. Phys., 2020, 127, 201101.
- 34 B. D. Fairbanks, M. P. Schwartz, A. E. Halevi, C. R. Nuttelman, C. N. Bowman and K. S. Anseth, Adv. Mater., 2009, 21, 5005-5010.
- 35 J. L. Leight, D. L. Alge, A. J. Maier and K. S. Anseth, Biomaterials, 2013, 34, 7344-7352.
- 36 J. A. McGlynn and K. M. Schultz, Macromolecules, 2022, 55, 4469-4480.
- 37 A. S. Rowlands, P. A. George and J. J. Cooper-White, Am. J. Physiol.: Cell Physiol., 2008, 295, C1037-C1044.
- 38 A. D. Lynn, A. K. Blakney, T. R. Kyriakides and S. J. Bryant, J. Biomed. Mater. Res., Part A, 2011, 96, 621-631.
- 39 E. M. Furst and T. M. Squires, Microrheology, Oxford University Press, 2017.
- 40 K. M. Schultz and E. M. Furst, Soft Matter, 2012, 8, 6198-6205.
- 41 T. G. Mason and D. A. Weitz, Phys. Rev. Lett., 1995, 74, 1250.
- 42 T. G. Mason, K. Ganesan, J. H. Van Zanten, D. Wirtz and S. C. Kuo, Phys. Rev. Lett., 1997, 79, 3282.
- 43 J. Hafner, D. Grijalva, A. Ludwig-Husemann, S. Bertels, L. Bensinger, A. Raic, J. Gebauer, C. Oelschlaeger, M. Bastmeyer and K. Bieback, et al., Acta Biomater., 2020, 111, 254-266.
- 44 M. S. Mazzeo, T. Chai, M. Daviran and K. M. Schultz, ACS Appl. Bio Mater., 2018, 2, 81-92.
- 45 M. P. Lutolf, J. L. Lauer-Fields, H. G. Schmoekel, A. T. Metters, F. E. Weber, G. B. Fields and J. A. Hubbell, Proc. Natl. Acad. Sci. U. S. A., 2003, 100, 5413-5418.
- 46 J. L. West and J. A. Hubbell, Macromolecules, 1999, 32, 241-244.
- 47 B. D. Fairbanks, M. P. Schwartz, C. N. Bowman and K. S. Anseth, Biomaterials, 2009, 30, 6702-6707.

- 48 T. G. Mason, Rheol. Acta, 2000, 39, 371-378.
- 49 T. M. Squires and T. G. Mason, Annu. Rev. Fluid Mech., 2010, 42, 413-438.
- 50 J. C. Crocker and D. G. Grier, J. Colloid Interface Sci., 1996, **179**, 298-310.
- 51 D. Adolf and J. E. Martin, Macromolecules, 1990, 23, 3700-3704.
- 52 K. M. Schultz and K. S. Anseth, Soft Matter, 2013, 9, 1570-1579.
- 53 T. Larsen, K. M. Schultz and E. M. Furst, Korea-Australia Rheology J., 2008, 20, 165-173.
- 54 T. Savin and P. S. Doyle, Biophys. J., 2005, 88, 623-638.
- 55 D. Dikovsky, H. Bianco-Peled and D. Seliktar, Biophys. J., 2008, 94, 2914-2925.

- 56 T. Yeung, P. C. Georges, L. A. Flanagan, B. Marg, M. Ortiz, M. Funaki, N. Zahir, W. Ming, V. Weaver and P. A. Janmey, Cell Motil. Cytoskeleton, 2005, 60, 24-34.
- 57 C. Bakal, J. Aach, G. Church and N. Perrimon, Science, 2007, 316, 1753-1756.
- 58 M. Ehrbar, A. Sala, P. Lienemann, A. Ranga, K. Mosiewicz, A. Bittermann, S. Rizzi, F. E. Weber and M. Lutolf, Biophys. J., 2011, **100**, 284-293.
- 59 R. Sunyer and X. Trepat, Curr. Biol., 2020, 30, R383-R387.
- 60 L. G. Vincent, Y. S. Choi, B. Alonso-Latorre, J. C. del Álamo and A. J. Engler, Biotechnology, 2013, 8, 472-484.
- 61 M. Daviran, H. S. Caram and K. M. Schultz, ACS Biomater. Sci. Eng., 2018, 4, 468-472.
- 62 M. Daviran and K. M. Schultz, Rheol. Acta, 2019, 1-17.